HYDROGEN SAFETY

Reduced Order Models for Liquid Hydrogen Pooling and Vaporization Supported by Experiments

RESEARCH

ETHAN S. HECHT

KIT Scientific Publishing

hySafe
INTERNATIONAL ASSOCIATION FOR HYDROGEN SAFETY

ABSTRACT

In the event of a leak of liquid hydrogen, a pool can form that vaporizes, disperses, and eventually dilutes to a non-flammable mixture. In this work, we describe fast-running models for the pooling and vaporization of liquid hydrogen in a steady cross-wind. Several pooling models from the literature are compared to solve for the flow and extent of the pool. The size of the pool can serve as the source for a separate dispersion model, which builds upon the existing one-dimensional Gaussian plume model in HyRAM+. Additional terms for the effects of a cross-wind on momentum and entrainment were added so that the model could handle the effects of a cross-wind on a low-speed flow. The models are compared to experimental data on pooling extent and downwind dispersion for steady flow rates of liquid hydrogen in a steady cross-wind. In the two compared experiments, liquid flow rates of 15 and 45 g/s were spilled onto concrete in cross-winds of approximately 1.8 m/s. The rate of growth of the pool and the downwind concentration boundaries are compared to the models, showing good agreement, although additional tuning is needed. These models can contribute to the advancement of codes and standards for liquid hydrogen systems.

CORRESPONDING AUTHOR:
Ethan S. Hecht
Hydrogen and Materials Science, Sandia National Laboratories, P.O. Box 969, MS 9052, Livermore, CA 94551, USA
ehecht@sandia.gov

KEYWORDS:
liquid hydrogen; pool; dispersion; model; experiment

TO CITE THIS ARTICLE:
Hecht, E.S. (2026). 'Reduced Order Models for Liquid Hydrogen Pooling and Vaporization Supported by Experiments'. *Hydrogen Safety*, 3(1), pp. 212–223. Available at: https://doi.org/10.58895/hysafe.70

DOI: 10.58895/hysafe.70

1. INTRODUCTION

Hydrogen is only a liquid at very low temperatures (approximately 20 K at 1 atmosphere), and if it spills onto a surface, it rapidly absorbs heat from its surroundings, vaporizes and disperses in the atmosphere. Understanding and modeling this type of release is important; to safely utilize this fuel, it is essential to understand where flammable regions occur so that ignition sources can be kept outside of these zones.

Thyer (2003) reviewed data on cryogenic liquid spills, noting only a single study with hydrogen (Takeno et al., 1994). Both the review and the study with hydrogen concluded that the boiling rate of liquid natural gas and hydrogen can often be correlated using a simple 1D heat-transfer conduction model with a boiling rate proportional to $t^{-1/2}$ (Thyer, 2003; Takeno et al., 1994). Friedrich et al. (2023) performed vaporization experiments on different substrates and similarly found a $t^{-1/2}$ boiling rate for liquid hydrogen spilled onto a solid surface. These studies had some confinement of the hydrogen in a vessel or with walls and did not examine the formation of a pool spreading on an unconfined surface.

Experiments by Royle and Willoughby (2014) observed an approximately 2.14 m long, 1.3 m wide pool for a downward release of liquid hydrogen onto concrete at 60 lpm from a 100 mm height in a 4 m/s cross-wind. The experiments were performed outdoors, so there was variability in the wind speed and direction. Some measurements of concentration demonstrated high variability, with occasional concentrations above 10 vol-% being observed 7.5 m downwind. Hansen and Hansen (2022) summarize experiments performed by the Norweigian Public Roads Administration (Aaneby et al., 2021). In outdoor tests, with 740 and 830 g/s releases downwards from 0.32 m height and wind speeds of approximately 4 and 2.5 m/s wind, temperatures below −200°C were observed at distances less than 0.5 m from the release point, and Hansen and Hansen (2022) claim little evidence of a pool, but Aaneby et al. (2021) describe a pool limited to 0.5 to 1 m from the release point. Indoor tests formed a pool 0.5–1 m from the release point with 500 g/s hydrogen spilling downwards onto the floor with very limited ventilation. In all cases, once the release stops, all remaining liquid quickly vaporizes. Although there have been a handful of other liquid hydrogen spill/release experiments (e.g., Arthur D. Little, Inc. (1960); Witcofski and Chirivella (1984); Schmidtchen et al. (1994); Verfondern and Dienhart (2007); Coldrick (2020); Buttner et al. (2021)), the data on liquid hydrogen spilling onto solid, unconfined surfaces, forming a pool, and dispersing into a cross-wind is quite limited.

Two common modeling approaches for pool formation and vaporization are solving the shallow water equations (Brandeis and Kansa, 1983; Brandeis and Ermak, 1983; Verfondern and Dienhart, 2007), or a simpler force balance driven by gravity (similar to the gas accumulation over spreading pools (GASP) approach of Webber (2012) and the model described by Nguyen et al. (2020)). Both of these approaches will result in a pool size over time, which is a function of the release rate and the heat transfer from the surface to the liquid being spilled, most often solved by assuming that solid surfaces can be treated as a semi-infinite (in depth).

Once the pool size and vaporization rate have been established, these details can be used as a source term for a dispersion model. Dispersion modeling can be accomplished using computational fluid dynamics or using simpler reduced-order models for dispersion. The Hydrogen Plus Other Alternative Fuels Risk Assessment Models (HyRAM+) (Ehrhart et al., 2024) toolkit has a plume dispersion model, but the current publicly released version does not have a model for wind effects, which are very important for these low momentum releases from a large pool. Wind will affect both the momentum and entrainment into the plume.

Experiential measurements of liquid hydrogen pooling and dispersion under well-controlled conditions have been made, and these are compared to newly developed reduced-order models in this work.

2. APPROACH

2.1 POOL MODELING

As discussed in the introduction, there are some common simplified models for pool formation and vaporization. An engineering model was developed by Cirrone et al. (2021) where a semi-infinite surface conducts heat into liquid hydrogen, driving vaporization at the same rate at

which the liquid hydrogen is flowing into the pool. The latent heat of vaporization, ΔH_{vap}, relates the mass flow rate m_{H_2} and the heat transfer, which is limited only to 1-D conduction from the surface (q_{cond}) through the relationship

$$\dot{m}_{H_2} = \frac{q_{cond}}{\Delta H_{vap}}. \tag{1}$$

The one-dimensional conduction to a semi-infinite surface can be analytically evaluated to

$$q_{cond} = \pi r_{pool}^2 \frac{k\left(T_{surface,\infty} - T_{boil}\right)}{\sqrt{\pi \alpha t}}, \tag{2}$$

where r_{pool} is the radius of the pool, k and α are the thermal conductivity and thermal diffusivity, respectively of the surface, $T_{surface,\infty}$ is the far-field (usually also the initial) temperature of the surface, and T_{boil} is the boiling point of the hydrogen at atmospheric pressure. Algebraic manipulation results in the pool radius as a function of time

$$r_{pool} = \sqrt{\frac{\dot{m}_{H_2} \Delta H_{vap}}{k\left(T_{surface,\infty} - T_{boil}\right)} \sqrt{\frac{\alpha t}{\pi}}}. \tag{3}$$

Inspection of this equation shows that the pool will continually grow at a rate proportional to $t^{1/4}$. This is due to the assumption of a semi-infinite solid with a constant temperature gradient at the surface (i.e., the use of Eq. 2) and the lack of other heat loss terms from the liquid hydrogen.

The second means of modeling the pool, colloquially called the GASP model, is a first-order system of differential equations described by Webber (2012):

$$\frac{dr}{dt} = u \tag{4}$$

$$\frac{du}{dt} = \frac{4gh(1-s)}{r} - F, \tag{5}$$

where r is the pool radius at time t, u is the velocity of the pool front, g is acceleration due to gravity, h is the height of the pool (assumed to be uniform), s is a shape factor that can be used to modify for non-solid surfaces (but is 0 for solid ground), and F is the frictional force of resistance to spreading. The height is related to the pool volume (assumed to be cylindrical) through the liquid hydrogen density and pool radius, while enforcing conservation of mass, which is given in Eq. 1 to close the system of equations. Conduction to the surface is calculated via Eq. 2, but the radius of the pool over time is tracked, with conduction integrated over the differential conduction annuli as the pool expands. Friction is calculated using the correlation from Webber (1991): the maximum of laminar ($F_{laminar}$) or turbulent ($F_{turbulent}$) frictional resistance is assumed where

$$F_{laminar} = 7.59 \frac{\nu u}{h^2} \tag{6}$$

$$F_{turbulent} = 4.49 C_f \frac{u^2}{h} \tag{7}$$

where ν is the dynamic viscosity of the liquid hydrogen, and C_f is a constant (assumed to be 1.69×10^{-3}). This system of equations was solved using an explicit Runge–Kutta method of order 8 implemented by SciPy (Virtanen et al., 2020).

Finally, the third means of modeling the pool in this work used the shallow water equations as described by several authors (Brandeis and Kansa, 1983; Brandeis and Ermak, 1983; Verfondern and Dienhart, 2007). The shallow water equations are a coupled set of first order partial differential equations with both time and radius as independent variables, where conservation of mass and momentum are written as

$$\frac{\partial (uh)}{\partial t} + \frac{\partial (urh)}{\partial r} + r(u - w) = 0 \tag{8}$$

$$\frac{\partial u}{\partial t} + \frac{\partial}{\partial r}\left(\frac{u^2}{2} + gh\right) + \frac{F}{h} = 0, \tag{9}$$

DOI: 10.58895/hysafe.70

where w is the vaporization velocity of the pool. Similar to the other models, the vaporization velocity is found by algebraically solving Eqs. 1 and 2, tracking the annular conduction over time. To use the ODE solver of SciPy (Virtanen et al., 2020), the domain is discretized in the radial dimension to 5000 points using upwinding and downwinding schemes suggested by Brandeis and Kansa (1983) before integrating the resulting system of ordinary differential equations over time using an explicit Runge–Kutta method of order 8 implemented by SciPy (Virtanen et al., 2020).

2.2 DISPERSION MODELING

The HyRAM+ model for jet dispersion was modified to include the effect of wind on momentum and entrainment. Details of the base model can be found in the HyRAM+ technical reference manual (Ehrhart et al., 2023), section 3.3.1. The effect on the momentum of the plume does not have any empirical coefficients. The streamwise derivative of the flow of momentum from the wind is equal to

$$\frac{d}{dS}\vec{p}_{wind} = \vec{v}_{wind}\rho_{ambient}E, \tag{10}$$

where S is the streamwise dimension, $\vec{p}_{wind}$ is the momentum flow vector from the wind [N], $\vec{v}_{wind}$ is the wind velocity vector [m/s], $\rho_{ambient}$ is the density of the ambient air [kg/m^3], and E is the entrained flow at a given streamwise point [m^2/s]. Components of this flow (by multiplying by the `sin` or `cos` of the relative wind angle) are added to the right-hand side of the appropriate x- and y-momentum equations (Eqs. 72 and 73 in Ehrhart et al. (2023)).

The effect of wind on entrainment has two empirical coefficients, a proportionality to the component of wind that is parallel to the flow direction ($c_{\parallel}$), and the component of the wind that is perpendicular ($c_{\perp}$). The entrained flow at each streamwise point is increased by

$$E_{wind} = B\left(c_{\perp}\left|v_{wind}\sin(\theta_{plume}-\theta_{wind})\right| + c_{\parallel}\left|v_{wind}\cos(\theta_{plume}-\theta_{wind}) - v_{plume,CL}\right|\right), \tag{11}$$

where E_{wind} is the additional entrainment due to wind [m^2/s] (added to Eq. 79 in Ehrhart et al. (2023)), B is the half-width of the plume [m], θ_{wind} and θ_{plume} are the angles of the wind and plume, respectively, to the x-axis, and $v_{plume,CL}$ is the centerline velocity of the plume, at each streamwise point.

The pool is assumed to be a circular source of saturated vapor hydrogen released vertically, and the HyRAM+ jet model with wind effects is used to solve for the trajectory. Manual experimentation with the effects of $c_{\parallel}$ and $c_{\perp}$ on the angle of the plume, compared to images of the visible cloud led to initial default values of $c_{\parallel} = 0.1$ and $c_{\perp} = 5$ being used in this work, although these values were varied for some simulations, as described later.

2.3 EXPERIMENTAL

Additional details can be found in Hecht (2025), but briefly, liquid hydrogen release experiments were performed in a large, repurposed blast tube where unimpeded pooling and dispersion could be simulated, but with a steady, controllable cross-wind. The blast tube has a 5.6 m diameter and a 115 m length. A large industrial fan, with filters a short distance downwind to prevent dust and provide a more uniform flow field, was able to produce steady cross-winds ranging from 0.9 to 1.9 m/s. Liquid hydrogen was staged in batches in a 1,500 l vacuum-insulated dewar that sat on top of a scale. The pressure in the dewar was maintained near atmospheric pressure and flowed, primarily due to gravity, into approximately the center of the blast tube. The hydrogen was released from 3 cm diameter piping approximately 23 cm above an interchangeable substrate, which was an approximately 1.2 m square piece of concrete, concrete with embedded thermocouples, or carbon steel. The spill rate was measured in two ways: based on the liquid level, which was calculated based on the differential liquid/vapor pressure in the dewar, and based on the mass loss rate detected by the scale upon which the dewar sat.

A grid of 7 × 7 (spaced by 15 cm) 1.3 mm diameter type-K thermocouples (without the central thermocouple so that the flow wouldn't be impeded) sat on top of the substrate to measure the extent of flow of liquid hydrogen. Due to the coarseness of the thermocouple grid, the limited

DOI: 10.58895/hysafe.70

accuracy of the thermocouples at low temperature, and potential time lag for cooling, any temperature observed below −220 °C (53 K) was assumed to be liquid hydrogen. Downwind of the pool, three movable rakes contained an additional 54 thermocouples. Co-located with 15 of the thermocouples were extractive tubes that were connected to the National Laboratory of the Rockies (NLR)'s hydrogen wide area monitoring (HyWAM) system (Buttner et al., 2021). Analysis elsewhere (Hecht, 2025) showed that the HyWAM measurements of mole fraction were well-correlated with the thermocouple measurements when adiabatic mixing of ambient air with saturated vapor hydrogen was assumed. For this work, the temperature measurements were converted to concentration for comparison to modeling results of mole fraction.

3. RESULTS AND DISCUSSION

The substrates in the experiments were small for some of the tests and liquid hydrogen could be observed spilling off of them, for high flow rates of liquid hydrogen. For comparisons to the extent of the pool, a test with a low flow rate of hydrogen was used. Example test results with a low hydrogen flow rate are shown in Figure 1. The green dashed vertical lines in Figure 1(a) show the time that the liquid hydrogen began to flow, just after 15:40. The gray shaded region shows the near steady-state data that was averaged, approximately 23.5 min. The red dashed vertical lines indicate the time when the liquid hydrogen stopped flowing. The top frame shows the pressure in the tank, which was slightly above atmospheric and decreased slightly as the

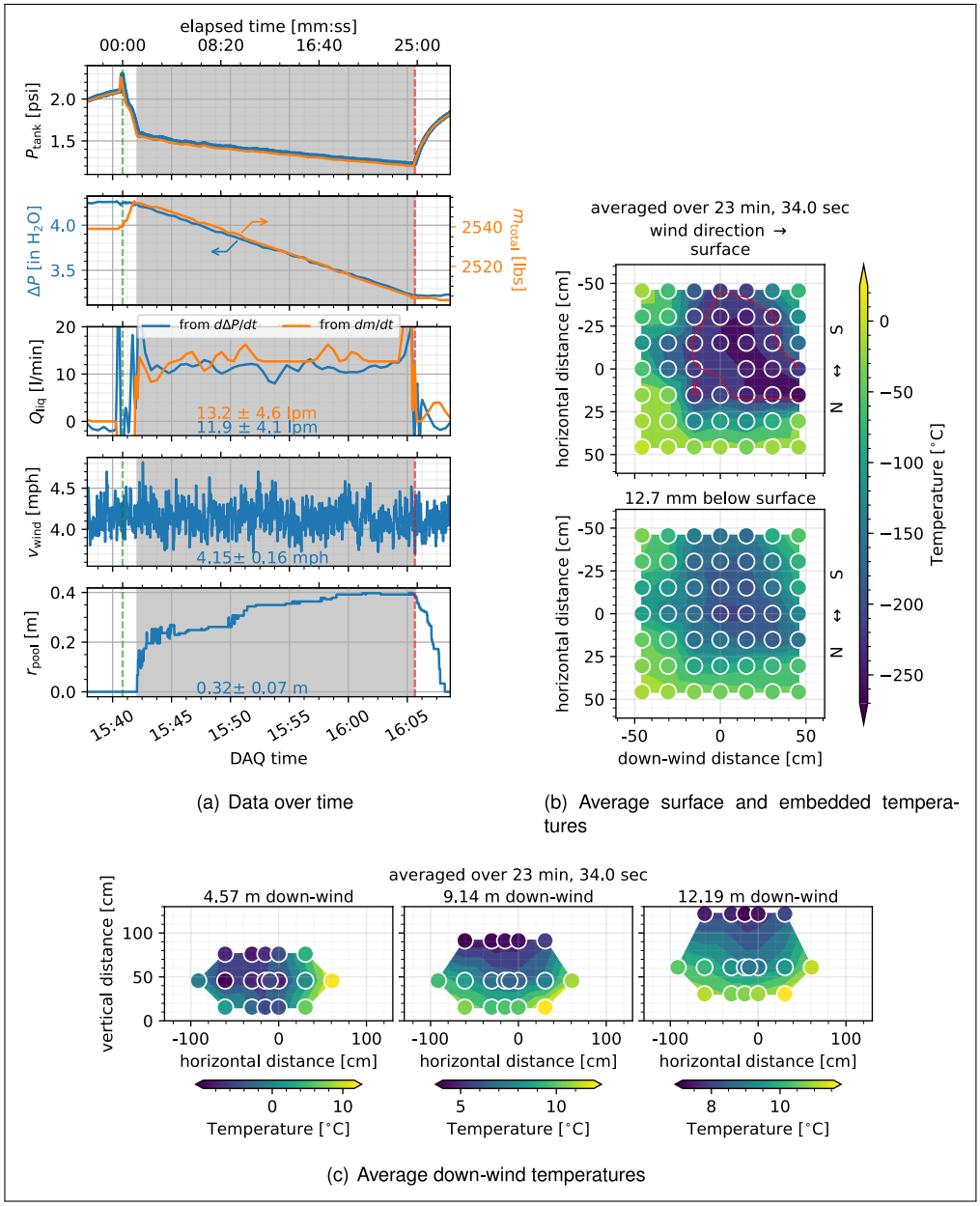

Figure 1 Experimental results for a 12.5 lpm release of LH_2 onto concrete with a 4 mph cross-wind.

DOI: 10.58895/hysafe.70

spill progressed. The second frame shows the two measurements that were converted into a volumetric flow rate, which is plotted in the third frame. Averaging the two measurements results in an approximate flow rate of 12.5 liters/minute (lpm) of hydrogen. The fourth frame down on the left shows the wind speed, which was approximately 1.9 m/s (4.15 mph), and the fifth frame shows the growth of the pool radius.

The contour plots in Figure 1(b) are average measurements of the temperatures at the surface (top) and 12.7 mm below the surface (bottom). The pool radius at each point in time was calculated from the instantaneous surface temperature measurements. Any temperatures below 53 K were assumed to be liquid hydrogen, and the area that was covered by liquid hydrogen was converted into a circular radius dimension. The red line shown in the upper plot of Figure 1(b) shows an approximate isocontour at 53 K; the approximate dimensions of the average pool. The pool is not centered on the substrate, but is being blown down-wind slightly and seems to flow in the southern/negative horizontal direction, perhaps due to a slight slope to that side, or an unevenness of the wind.

The three contour plots in Figure 1(c) show the average down-wind thermocouple temperatures at three down-wind locations. Temperatures are lowest towards the middle and top of the measurements, and also increase going downwind (note the different temperature scales for each of the frames). Because the flow rate of hydrogen was so low, the temperatures are fairly close to ambient (at the edges of the plots); in other words, the mole fraction of hydrogen is low.

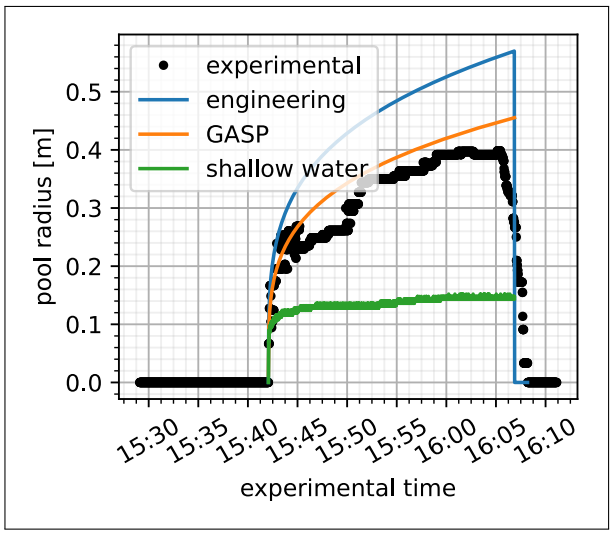

Figure 2 Experimental data of pool radius for the test shown in Figure 1 (12.5 lpm liquid hydrogen flow) compared to the different pooling models for concrete with properties of $k = 1.4$ W/m-K, $\alpha = 6.9 \times 10^{-7}$ m^2/s.

Figure 2 compares the three different pooling modeling approaches to the data from the experiment of Figure 1. The blue line shows the result of the engineering model described by Eq. 3. The engineering model predicts the largest pool of the three models, and overpredicts the radius in this case. The orange line is the result of the GASP model, described by Eqs. 4 and 5. With the properties used, however, there were issues getting the ODE solver to converge, and the frictional force needed to be increased by a factor of 15 to get the model to integrate. Nonetheless, the radius predicted is very near the experimental results. Finally, the shallow water equations, given in Eqs. 8 and 9, result in a prediction of pool radius that is much smaller than was observed experimentally. Other simulations using these models (not shown) showed similar trends of the engineering model always predicting the largest pool radius, the shallow water equations the smallest, and the GASP model somewhere in-between. The GASP and shallow water equations are both currently slow to solve due primarily to tracking the pool radius over time to determine the annular conductive heat flux. Additional work on the models is needed to increase the speed of solutions, and hopefully improve the range of material properties (e.g., substrate conductivity, substrate thermal diffusivity) for which a solution can be found.

Since there are challenges in predicting the pool radius over time, and previous work showed that CFD models for dispersion were relatively insensitive to the pool radius (Mangala Gitushi et al., 2023), the dispersion model was tested for its sensitivity to pool radius. The left-hand

DOI: 10.58895/hysafe.70

frames of Figure 3 show the 4% mole fraction contour for a 1 m diameter source pool, and the right-hand frames for a 0.5 m diameter source pool for two hydrogen flowrates and 3 wind speeds. A red dashed line on the plot also shows the vector to the tip of the 4% mole fraction contour and the angle of that line is shown in red text. Aside from the bulging contour near the plume origin ($x < 0$), the contours are nearly identical. The bulge is an artifact of displaying the plume as its trajectory rotates from the vertical release to the nearly horizontal wind-driven dispersion near the pool source, while it is diluted greatly by wind-driven entrainment. In a real release, one would expect the average mole fraction contour to be smooth all the way down to the pool. The larger pool has a barely perceptible longer profile in the x-dimension. A higher flow rate of liquid hydrogen results in a more upward-driven plume (it starts with additional upward momentum), and also results in a longer plume with more flammable mass contained within.

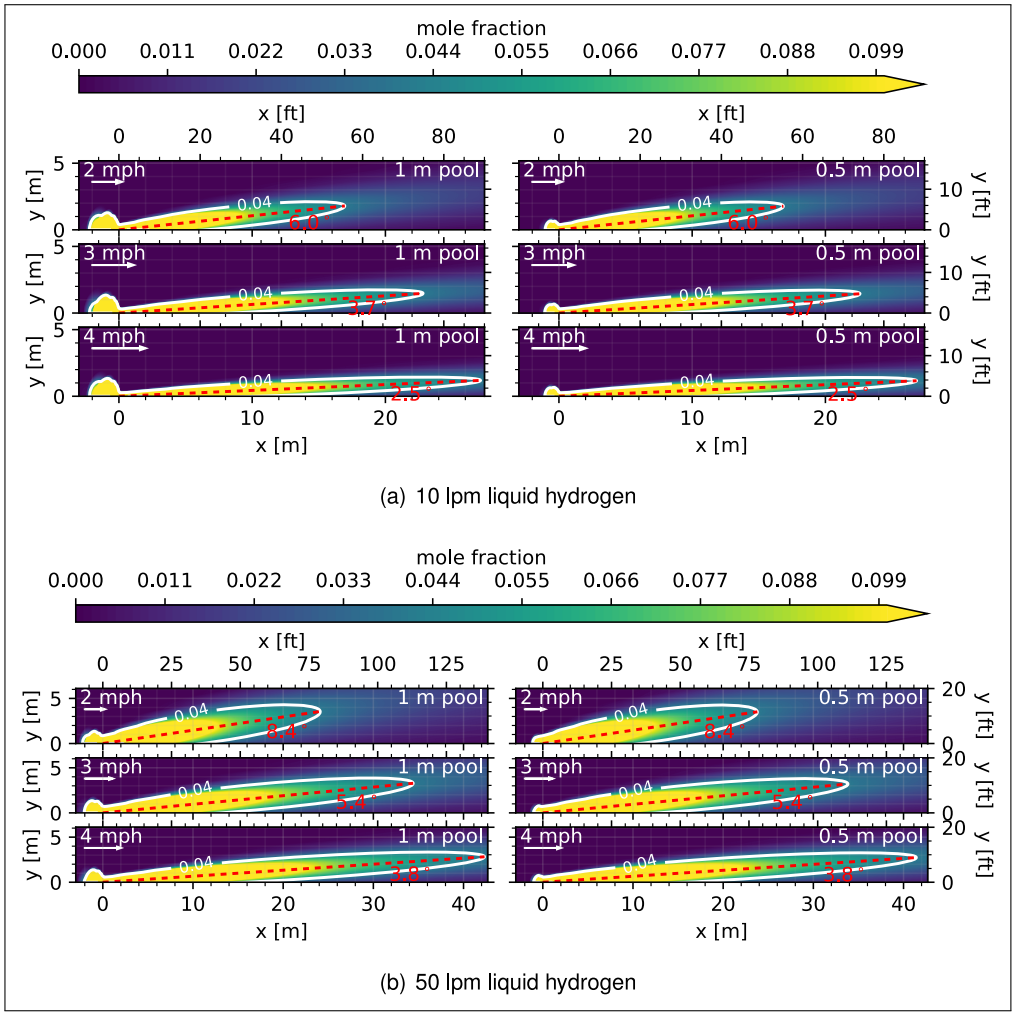

Figure 3 HyRAM+ dispersion model with variations in wind speed (rows) and source pool diameter (columns).

Due to uncertainty with the pool model (and the independence of plume dispersion on the pool radius), the dispersion model was compared to experimental data using an average experimentally measured pool radius as the source of hydrogen. The experimentally measured average mass flow rate and wind speed were also used in the model. The wind was given an upward trajectory of 5° above horizontal because the experimental configuration had a ramp leading up to the substrate that was not directly on the ground. Figure 4 shows the experimental data compared to the HyRAM+ model for two experiments with different release rates of liquid hydrogen of 15 and 45 g/s. Both the data and the model contain upward sloping plumes, and the high mole fractions extend further downwind as the hydrogen release rates increase. However, the mole fractions predicted by the model are much higher than those observed experimentally; there is much more spreading and dilution in reality than is predicted by the model. A more diluted, wider plume is also clear from the side profiles. In particular, Figure 4(a) shows an entire simulated mole fraction field that is less than 0.04 for the slice that is −61 cm from the center. The experimental plume, on the other hand,

has mole fractions that are greater than 0.08, at least in the part of the slice that is 4.57 m downwind of the pool. The profiles further show that the average experimental plume is not centered on the axis. Video evidence also showed that the condensed moisture tilted in the negative horizontal direction. Obstructions (such as cameras and data acquisition equipment) upwind of the release are suspected of causing the wind to deviate slightly from the blast tube axis.

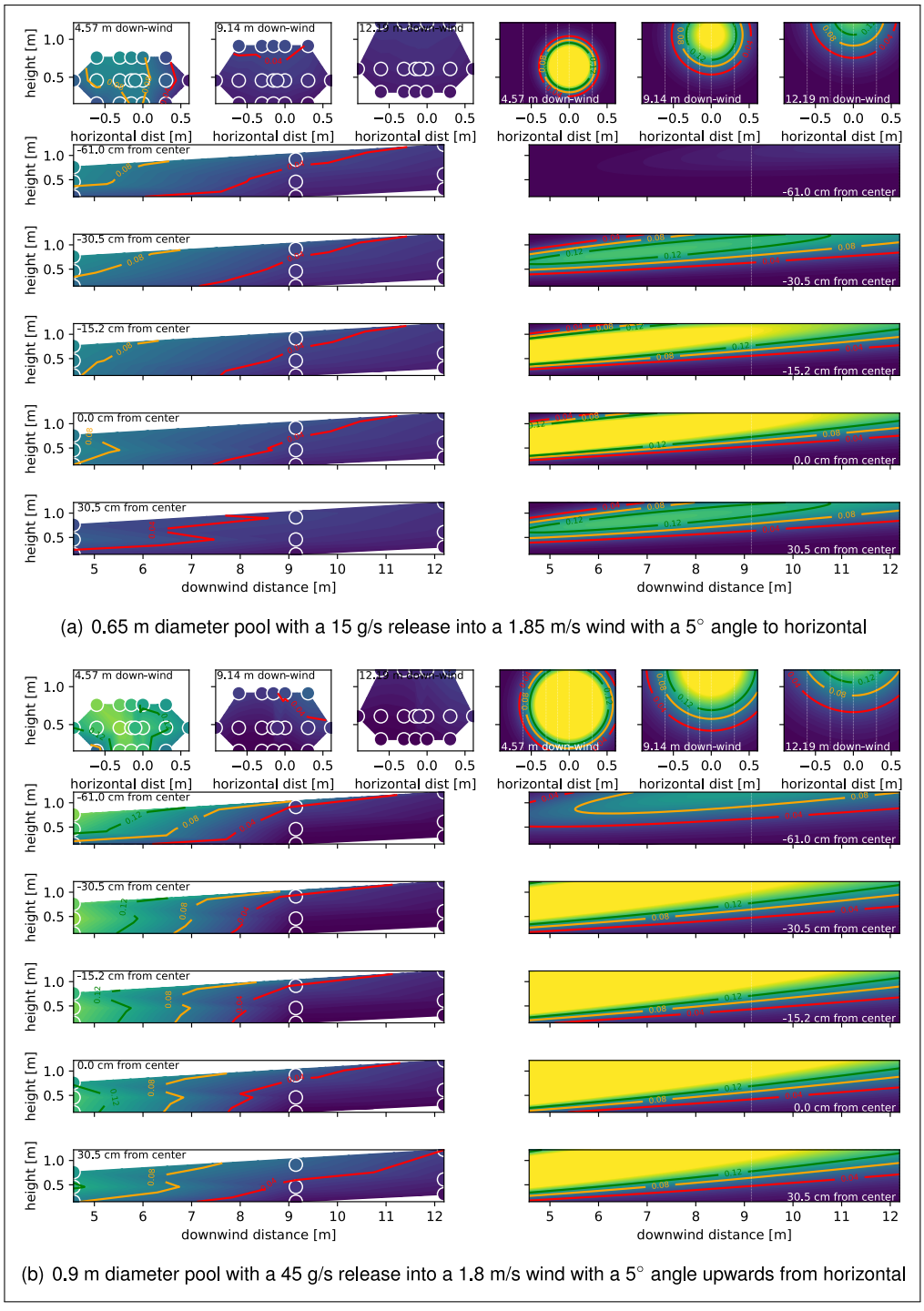

Figure 4 Experimental data (left) compared to HyRAM+ dispersion model (right) for two different conditions. Top row contains slices in the downwind direction and bottom 5 frames are the same data, but sliced in the horizontal direction.

The amount of dilution in the model is easily controlled by the entrainment coefficients, $c_{\|}$ and $c_{\perp}$. In Figure 5, both $c_{\|}$ and $c_{\perp}$ were varied, to 0.9 and 1.8, respectively. In this case, the extent of the plume and mole fractions are significantly reduced, and the plume is much wider, but the upward trajectory of the plume is also reduced. As the entrainment of air increases (due to the significant increase in $c_{\|}$), the buoyancy of the plume decreases, since hydrogen is the buoyant component of the plume, and if there is less hydrogen in the plume, there is commensurately less buoyancy. A thorough comparison and automated minimization of error between the model results and all of the experimental data with additional flow rates

of hydrogen, additional cross-wind speeds, and other substrates are needed to see if additional tuning of the entrainment coefficients can improve the agreement between the model and the data.

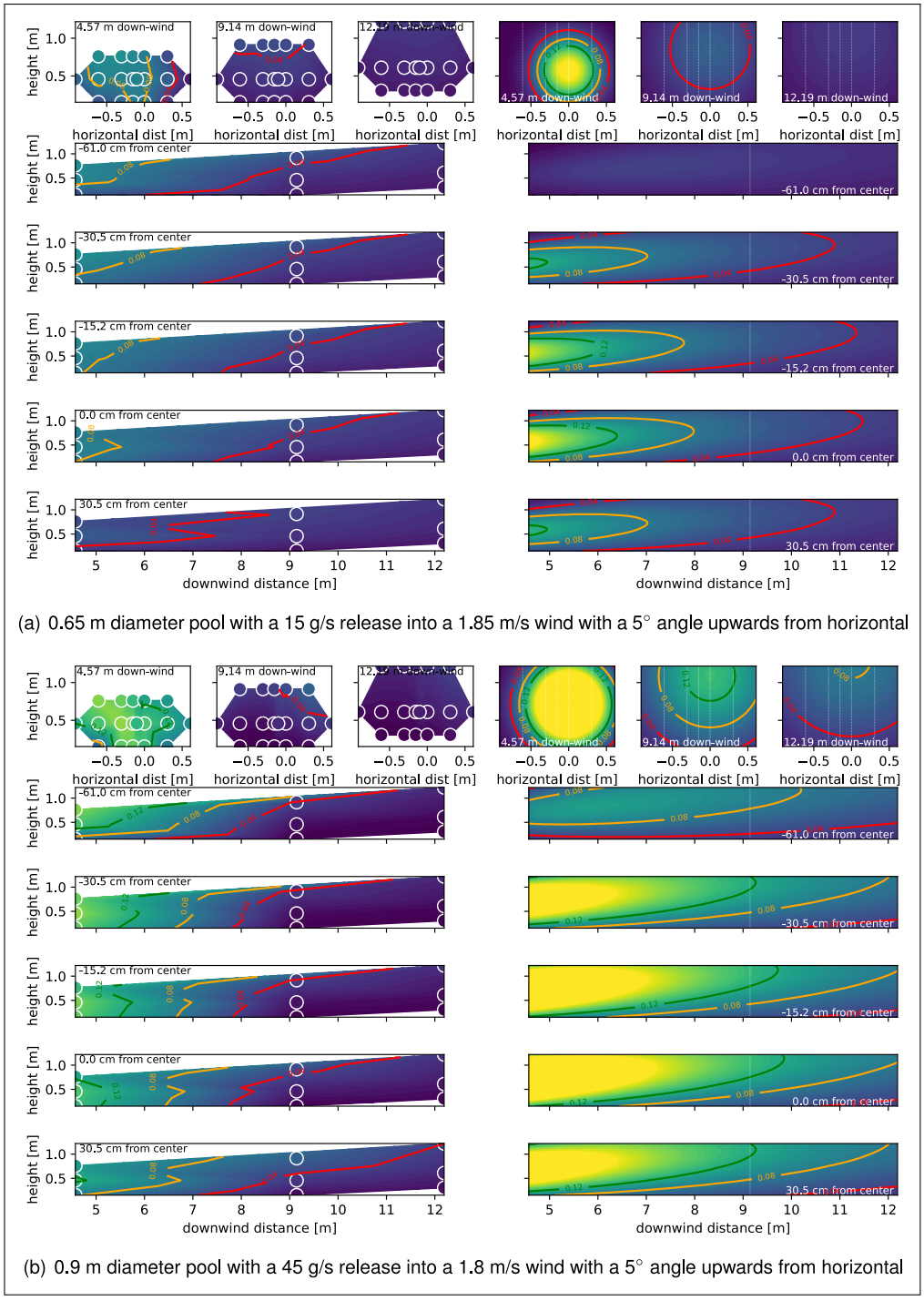

(a) 0.65 m diameter pool with a 15 g/s release into a 1.85 m/s wind with a 5° angle upwards from horizontal

(b) 0.9 m diameter pool with a 45 g/s release into a 1.8 m/s wind with a 5° angle upwards from horizontal

Figure 5 Experimental data (left) compared to HyRAM+ dispersion model (right) for two different conditions, with entrainment coefficients changed to $c_{\parallel} = 0.9$ and $c_{\perp} = 1.8$. Top row contains slices in the downwind direction and bottom 5 frames are the same data, but sliced in the horizontal direction.

4. SUMMARY AND CONCLUSIONS

Three different models for pool formation over time are described in this work. An algebraic engineering model overpredicted the pool radius over time; the GASP approach seemed to agree with the experimental data, while a solution of the shallow water equations underpredicted the experimentally observed pool radius. The GASP approach and the shallow water equations have issues with solution stability for certain scenarios and are also slow to solve. Both of these models need additional work to address these deficiencies.

A fast-running dispersion model that is an extension of a plume model in HyRAM+ is also described in this work. The HyRAM+ plume model was modified to include the effects wind

has on the momentum of a plume, as well as how wind affects the entrainment of air into the plume. The pool radius is an input to the plume model, and it was demonstrated that the pool radius has little effect on the downwind dispersion of the plume, at least for the limited pool radii (0.5 m versus 1 m) and low winds (< 4 mph) tested in this work. This means that the accuracy of the pool formation is not critical to understanding the dispersion of vaporizing liquid hydrogen spills.

The dispersion model was then exercised, using parameters and data from two different experimental spill rates of liquid hydrogen onto concrete, to assess the accuracy of the model. With the initial empirical coefficients for wind entrainment, the predicted mole fractions were much higher than those observed experimentally. Increasing the parallel driven entrainment coefficient lowered the predicted mole fractions, but also decreased the predicted buoyancy of the simulated plumes. The agreement with the data was improved slightly, but the model needs additional tuning.

In future work, the pooling model will be linked more closely with the dispersion model, and additional optimization of the entrainment coefficients will be made. The optimization will be automated and will use the entire dataset from the pooling experiments that were performed, which includes additional variations in wind speed, spill rate, and substrate beyond what is presented in this work. In addition to the vaporization data presented in this work, literature data will also be used to determine the entrainment coefficients. It is possible that the entrainment coefficients are not simple values but are a function of the experimental parameters, as is the case for momentum and buoyancy-driven entrainment in the HyRAM+ model. This model will be incorporated into the HyRAM+ toolkit and will be useful in assessing the safety of liquid hydrogen systems and the characteristics of specific scenarios that involve spills of liquid hydrogen in an open environment with a cross-wind.

ACKNOWLEDGEMENTS

The author is extremely grateful to the entire experimental team, including Walt Gill who started as the test director in New Mexico before he retired, and Victor Figueroa, who took over as the test director. The testing couldn't have been done with the amazing technologists, led by Carl Fitzgerald, with Shane Adee, Daniel Roybel, and Seth Spitzer providing tremendous support throughout the project and especially during the test week. The photometrics crew was also fantastic, led by Alvaro Cruz-Cabrera, with Bryon Demosthenous and Caleb Heine. The author is also grateful to Kyle Winter and the team at Thunder Range for their support of this project. Staff from Chart Industries, especially Tom Drube, and from Air Products, especially Dave Farese and Jeremiah Crosier, were instrumental in helping evaluate and improve the experimental design. Thanks to Bill Buttner and James Stewart from the National Laboratory of the Rockies (NLR) for providing the Hydrogen Wide Area Monitoring system, especially James who was onsite for testing to run the system.

FUNDING INFORMATION

This material is based on work supported by the U.S. Department of Energy's Office of Critical Minerals and Energy Innovation (CMEI) under the Alternative Fuels and Feedstocks Office (AFFO), formerly the Hydrogen and Fuel Cell Technologies Office (HFTO). Sandia National Laboratories is a multi-mission laboratory managed and operated by National Technology & Engineering Solutions of Sandia, LLC (NTESS), a wholly owned subsidiary of Honeywell International Inc., for the U.S. Department of Energy's National Nuclear Security Administration (DOE/NNSA) under contract DE-NA0003525. This written work is authored by an employee of NTESS. The employee, not NTESS, owns the right, title, and interest in and to the written work and is responsible for its contents. Any subjective views or opinions that might be expressed in the written work do not necessarily represent the views of the U.S. Government. The publisher acknowledges that the U.S. Government retains a non-exclusive, paid-up, irrevocable, worldwide license to publish or reproduce the published form of this written work or allow others to do so, for U.S. Government purposes. The DOE will provide public access to results of federally sponsored research in accordance with the DOE Public Access Plan.

COMPETING INTERESTS

The author has no competing interests to declare.

AUTHOR CONTRIBUTIONS

Ethan Hecht developed and implemented the models, led the experimental campaign, analyzed data, and authored this work.

AUTHOR AFFILIATIONS

Ethan S. Hecht orcid.org/0000-0001-8380-9072
Hydrogen and Materials Science, Sandia National Laboratories, P.O. Box 969, MS 9052, Livermore, CA 94551, USA

REFERENCES

Aaneby, J., Gjesdal, T. and **Voie, O.** (2021) *Large scale leakage of liquid hydrogen (LH2) – tests related to bunkering and maritime use of liquid hydrogen.* Technical Report FFI-RAPPORT 20/03101, Norwegian Defence Research Establishment (FFI). Available at: https://www.ffi.no/en/publications-archive/large-scale-leakage-of-liquid-hydrogen-lh2-tests-related-to-bunkering-and-maritime-use-of-liquid-hydrogen

Arthur D. Little, Inc. (1960) *Final report on an investigation of hazards associated with the storage and handling of liquid hydrogen.* Technical Report C-61092, Air Force Ballistic Missile Division.

Brandeis, J. and **Ermak, D.L.** (1983) 'Numerical simulation of liquefied fuel spills: II. Instantaneous and continuous lng spills on an unconfined water surface', *International Journal for Numerical Methods in Fluids*, 3(4), pp. 347–361. Available at: https://doi.org/10.1002/fld.1650030405

Brandeis, J. and **Kansa, E.J.** (1983) 'Numerical simulation of liquefied fuel spills: I. Instantaneous release into a confined area', *International Journal for Numerical Methods in Fluids*, 3(4), pp. 333–345. Available at: https://doi.org/10.1002/fld.1650030404

Buttner, W., Hall, J., Coldrick, S., Hooker, P. and **Wischmeyer, T.** (2021) 'Hydrogen wide area monitoring of LH2 releases', *International Journal of Hydrogen Energy*, 46(23), pp. 12497–12510. Available at: https://doi.org/10.1016/j.ijhydene.2020.08.266

Cirrone, D., Makarov, D., Molkov, V., Venetsanos, A., Coldrick, S., Atkinson, G., Proust, C., Friedrich, A. and **Kuznetsov, M.** (2021) Detailed description of novel engineering correlations and tools for LH2 safety, version 2. Technical Report D6.5, Pre-normative REsearch for Safe use of Liquid Hydrogen (PRESLHY). Available at: https://hysafe.info/wp-content/uploads/sites/3/2021/04/210429_PRESLHY_D6.5_Version2.1_Final.pdf

Coldrick, S. (2020) *PRESLHY WP3–rainout in large scale LH2 releases.* Available at: https://hysafe.info/wp-content/uploads/sites/3/2021/05/3_4_Coldrick_Rainout_HSE_v2.pdf (Accessed: 2025-05-12).

Ehrhart, B., Hecht, E. and **Schroeder, B.** (2023) Hydrogen plus other alternative fuels risk assessment models (HyRAM+) version 5.1 technical reference manual. Technical Report SAND2023-14224, Sandia National Laboratories. Available at: https://doi.org/10.2172/2369637

Ehrhart, B.D., Sims, C., Hecht, E.S., Schroeder, B.B., Liu, B.R., Groth, K.M., Reynolds, J.T. and **Walkup, G.W.** (2024) HyRAM+ (hydrogen plus other alternative fuels risk assessment models), version 5.1.1. Available at: https://hyram.sandia.gov

Friedrich, A., Breitung, W., Veser, A., Kuznetsov, M., Gerstner, J. and **Jordan, T.** (2023) Liquid hydrogen pool evaporation above four different substrates. In *Proceedings of the 2023 International Conference on Hydrogen Safety*. Available at: https://hysafe.info/uploads/papers/2023/290.pdf

Hansen, O.R. and **Hansen, E.S.** (2022) 'CFD-modelling of large scale LH2 release experiments', *Chemical Engineering Transactions*, 90, pp. 619–624.

Hecht, E.S. (2025) Liquid hydrogen pooling and vaporization experiments. Technical Report SAND2025-08847, Sandia National Laboratories. Available at: https://doi.org/10.2172/2585576

Mangala Gitushi, K., Blaylock, M. and **Hecht, E.S.** (2023) 'Simulations for planning of liquid hydrogen spill test', *Energies*, 16(4), p. 1580. Available at: https://doi.org/10.3390/en16041580

Nguyen, L.D., Kim, M., Choi, B., Chung, K., Do, K. and **Kim, T.** (2020) 'An evaluation of vaporization models for a cryogenic liquid spreading on a solid ground', *International Journal of Heat and Mass Transfer*, 146, p. 118848. Available at: https://doi.org/10.1016/j.ijheatmasstransfer.2019.118848

Royle, M. and **Willoughby, D.** (2014) *Releases of unignited liquid hydrogen.* Technical Report RR986, Health and Safety Executive. Available at: https://www.hse.gov.uk/research/rrhtm/rr986.htm

Schmidtchen, U., Marinescu-Pasoi, L., Verfondern, K., Nickel, V., Sturm, B. and **Dienhart, B.** (1994) 'Simulation of accidental spills of cryogenic hydrogen in a residential area', *Cryogenics*, 34, pp. 401–404. Available at: https://doi.org/10.1016/S0011-2275(05)80091-8

Takeno, K., Ichinose, T., Hyodo, Y. and **Nakamura, H.** (1994) 'Evaporation rates of liquid hydrogen and liquid oxygen spilled onto the ground', *Journal of Loss Prevention in the Process Industries*, 7(5), pp. 425–431. Available at: https://doi.org/10.1016/0950-4230(94)80061-8

Thyer, A. (2003) 'A review of data on spreading and vaporisation of cryogenic liquid spills', *Journal of Hazardous Materials*, 99(1), pp. 31–40. Available at: https://doi.org/10.1016/S0304-3894(02)00355-2

Verfondern, K. and **Dienhart, B.** (2007) 'Pool spreading and vaporization of liquid hydrogen', *International Journal of Hydrogen Energy*, 32(13), pp. 2106–2117. Available at: https://doi.org/10.1016/j.ijhydene.2007.04.015

Virtanen, P., Gommers, R., Oliphant, T.E., Haberland, M., Reddy, T., Cournapeau, D., Burovski, E., Peterson, P., Weckesser, W., Bright, J., van der Walt, S.J., Brett, M., Wilson, J., Millman, K.J., Mayorov, N., Nelson, A.R.J., Jones, E., Kern, R., Larson, E., Carey, C.J., Polat, İ., Feng, Y., Moore, E.W., VanderPlas, J., Laxalde, D., Perktold, J., Cimrman, R., Henriksen, I., Quintero, E.A., Harris, C.R., Archibald, A.M., Ribeiro, A.H., Pedregosa, F., van Mulbregt, P. and **SciPy 1.0 Contributors** (2020) 'SciPy 1.0: fundamental algorithms for scientific computing in Python', *Nature Methods*, 17, pp. 261–272. Available at: https://doi.org/10.1038/s41592-020-0772-5

Webber, D. (1991) 'Source terms', *Journal of Loss Prevention in the Process Industries*, 4(1), pp. 5–15. Available at: https://doi.org/10.1016/0950-4230(91)80002-C

Webber, D. (2012) 'On models of spreading pools', *Journal of Loss Prevention in the Process Industries*, 25(6), pp. 923–926. Available at: https://doi.org/10.1016/j.jlp.2012.05.003

Witcofski, R.D. and **Chirivella, J.** (1984) 'Experimental and analytical analyses of the mechanisms governing the dispersion of flammable clouds formed by liquid hydrogen spills', *International Journal of Hydrogen Energy*, 9(5), pp. 425–435. Available at: https://doi.org/10.1016/0360-3199(84)90064-8

TO CITE THIS ARTICLE:
Hecht, E.S. (2026). 'Reduced Order Models for Liquid Hydrogen Pooling and Vaporization Supported by Experiments'. *Hydrogen Safety*, 3(1), pp. 212–223. Available at: https://doi.org/10.58895/hysafe.70

Submitted: 07 March 2026
Accepted: 02 June 2026
Published: 16 June 2026

Hydrogen Safety is a peer-reviewed open access journal published by KIT Scientific Publishing.

KIT Scientific Publishing